

# NASA Technical Memorandum 58264

(NASA-TM-58264) DESIGN STUDY OF AN  
INTEGRATED AEROBRAKING ORBITAL TRANSFER  
VEHICLE (NASA) 40 p HC A03/MF A01 CSCL 22B

N85-21262

Unclas  
G3/20 15147

## Design Study of an Integrated Aerobraking Orbital Transfer Vehicle

March 1985

**NASA**

National Aeronautics and  
Space Administration

NASA Technical Memorandum 58264

Design Study of an Integrated Aerobraking  
Orbital Transfer Vehicle

Carl D. Scott, Barney B. Roberts, Kornel Nagy, Peter Taylor,  
Joe D. Gamble, Christopher J. Ceremeli, Kenneth R. Kroll,  
Chien P. Li, and Robert C. Ried

March 1985

National Aeronautics and Space Administration  
Lyndon B. Johnson Space Center  
Houston, Texas 77058

CONTENTS

Section	Page
ABSTRACT.....	1
INTRODUCTION.....	1
AEROASSIST BACKGROUND.....	2
VEHICLE CONCEPT AND GROUND RULES.....	6
GEOMETRICAL CONCEPT DESCRIPTION.....	7
AERODYNAMICS.....	7
VEHICLE CONCEPT.....	7
PROPULSION.....	8
VEHICLE STRUCTURE CONCEPT.....	9
STRUCTURAL MASS ESTIMATE.....	10
AEROBRAKING TRAJECTORY.....	10
AERODYNAMIC HEATING ESTIMATES.....	11
THERMAL PROTECTION.....	12
TOTAL VEHICLE MASS.....	12
PERFORMANCE.....	13
TECHNOLOGY IMPROVEMENTS.....	15
CONCLUSIONS.....	15
REFERENCES.....	32

TABLES

Table	Page
1 JSC AOTV CONFIGURATION MASS SUMMARY (GEO RETURN).....	16

~

PRECEDING PAGE BLANK NOT FILMED

## FIGURES

Figure	Page
1 Payload-to-stage mass ratio of all propulsive and aerobraked stages.....	17
2 Improvement in GEO delivery payload compared with aerobrake mass.....	18
3 Geometric construction of blunted, raked-off cone.....	19
4 Integrated AOTV design in aerobraking attitude.....	20
5 Newtonian aerodynamic coefficients of blunted, raked-off cone.....	21
6 Integrated AOTV concept with 12-m (40-ft) diameter heat shield.....	22
7 Side view of half-model AOTV heat shield structure and bulkheads.....	23
8 Front view of half-model of AOTV heat shield structure and bulkheads.....	24
9 Altitude time history during AOTV aerobraking.....	25
10 Velocity time history during AOTV aerobraking.....	26
11 AOTV atmospheric flight trajectory characteristics.....	27
12 AOTV atmospheric flight environment.....	28
13 Heat flux and pressure distributions on aerobrake referenced to stagnation point value.....	29
14 Computational body with Mach number contours in shock layer.....	30
15 Fractional increase of GEO delivery mass for aerobraked stage over an all propulsive stage.....	31

## ACRONYMS

AOTV	Aerobraking orbital transfer vehicle
EOM	End-of-mission
GEO	Geosynchronous Earth orbit
HRSI	High temperature re-useable surface insulation
LEO	Low Earth orbit
OTV	Orbital transfer vehicle
RCS	Reaction control system
RTV	Room temperature vulcanizing silicone rubber
TPS	Thermal protection system

## SYMBOLS

A	reference area
a	dimensionless ratio, $\Delta V / I_{sp} g_0$
$C_D$	drag coefficient
$C_L$	lift coefficient
$C_m$	pitching moment coefficient
$C_n$	yawing moment
$I_{sp}$	specific impulse of rocket
L/D	lift-to-drag ratio
M	Mach number
m	mass of vehicle at entry
q	heat flux
$R_N$	nose radius at stagnation point
$\bar{t}$	effective skin thin thickness
V	velocity

(4)

SYMBOLS CONTINUED

$W_{AB}$	weight penalty for aerodynamic and TPS surfaces
$W_{GEO}$	mass of payload delivered to GEO
$W_{GEOAP}$	payload mass to GEO by all propulsive stage
$W_{LEO}$	total departure mass from LEO to GEO
$W_P$	full propellant mass capacity
$W_S$	stage dry mass
$W_{SAB}$	aerobraked stage mass
$W_{SAP}$	propulsive stage mass
$W_f$	weight at end of burn
$W_i$	weight at start of burn
$\alpha$	angle of attack
$\beta$	side slip angle
$\delta$	rake angle
$\epsilon_b$	bluntness ellipticity
$\lambda$	mass fraction
$\rho$	density
$\theta$	cone angle

SUBSCRIPTS

AB, B	aerobrake
AP, P	all propulsive
$\infty$	freestream condition

## ABSTRACT

An aerobraking orbital transfer vehicle (AOTV) concept, which has an aerobrake structure that is integrated with the propulsion stage, is discussed. The conceptual vehicle is to be assembled in space and is space-based. The paper discusses the advantages of aeroassist over an all propulsive vehicle and indicates that the vehicle considered is very competitive with inflatable and deployable concepts from mass and performance aspects. The aerobrake geometry is an ellipsoidally blunted, raked-off, elliptical wide-angle cone with a toroidal skirt. Propellant tanks, engines, and subsystems are integrated into a closed, isogrid aerobrake structure which provides rigidity. The vehicle has two side-firing, gimballed RL-10 type engines connected by struts to a web bulkhead thrust structure.

The AOTV has 38 000 kg (84 000 lb) of useable propellant loaded into tanks and is sized to be carried in the Shuttle payload bay. One of the liquid hydrogen tanks is sized for just the descent to reduce boiloff. The trajectory during aerobraking is determined from an adaptive guidance logic, and the heating is determined from engineering correlations as well as 3-D Navier-Stokes solutions. A thermal protection system (TPS) consisting of high temperature surface insulation bonded to the skin of the aerobrake is sized for the expected aeroheating. The aerobrake structure and TPS are found to be approximately 17 percent of the total stage dry mass. The AOTV is capable of placing a 13 500 kg (29 800 lb) payload into geosynchronous Earth orbit (GEO) or carrying a LEO-GEO-LEO round-trip payload of 7100 kg (15 700 lb). A two-stage version considered for lunar missions results in a lunar surface delivery capability of 18 800 kg (41 500 lb) or a round-trip capability of 6800 kg (15 000 lb) with an additional 3860 kg (8500 lb) deliver-only capability. The dry mass of the stage is approximately 4430 kg (9760 lb) and the re-entry mass with a 6800 kg (15 000 lb) payload is 13 200 kg (29 000 lb).

## INTRODUCTION

As the Space Transportation System becomes an operational reality and the Nation addresses the challenge of permanent manned presence in space, it is appropriate to consider practical approaches toward the transport of systems, materials, and man beyond the low Earth orbit (LEO) region of the Space Station. Given the economy of the reusable Space Shuttle Orbiter, the energy requirements for leaving the Earth to achieve LEO are dear and not to be squandered. This, in conjunction with a Space Station in LEO, drives one toward consideration of space-based reusable vehicles designed to take advantage of a more specialized application. The vehicle should be versatile enough to meet mission requirements, but not carry the design burdens required for returning to the surface of the Earth or the energy expense of reboost to LEO. The achievement of this efficiency is not without investment. The design and development of space-based transportation systems entails challenge for the assembly, servicing, maintenance, check-out, loading of propellant and cargo, and all aspects of vehicle turnaround in an Earth orbital environment.

The second major energy efficiency to be considered is the use of atmospheric braking for the dissipation of relative energy upon return to LEO. This maneuver avoids using propellant masses which would otherwise be carried for a full mission, but requires the mass burdens of an aerobraking thermal protection system (TPS) and the design constraints of an acceptable aerodynamic configuration. The Mercury, Gemini, Apollo, and Space Shuttle Orbiter have used aerobraking to great advantage for return to Earth with the latter system having achieved this with a reuseable TPS system. The reuseable TPS feature is of great advantage for a space-based system, but more difficult as the relative velocity and the aerodynamic heating increase. Aerobraking to LEO is also significantly different from atmospheric entry achieved by previous manned spacecraft in that capture must be avoided. Thus, an aerobraking orbital transfer vehicle (AOTV) must fly between the limits of the atmosphere and a capture boundary as opposed to, for example, the Apollo vehicles which flew between a capture boundary and severe deceleration limits. Like the Space Shuttle Orbiter, an AOTV flight through the atmosphere must avoid excessive heating and must be consistent with the TPS capability and the aerodynamic performance requirements for achieving the maneuver.

The purpose of this paper is to project the potential characteristics of an AOTV by consideration of a particular or "point" design based on reasonable, but somewhat arbitrary guidelines. The attempt is to extrapolate slightly into the future based on the historic trends of both systems and technology. The value of this is fourfold. First, the concept of what a space-based AOTV might be like should help in consideration of the design and development of a Space Station, at which such a vehicle may be based. Second, the development of a propulsion system for an AOTV requires a concept of what the overall system might entail. Third, a base of vehicle characteristics predicted on a somewhat conservative approach of extrapolation from the past is needed to provide perspective on current and future innovative ideas and approaches. Finally, identification of potential system characteristics should help provide guidance for planning programs in related research and technology development.

In perspective, the design process does not provide unique solutions and seldom provides optimum solutions. Given the same guidelines as selected here, there are a large number of approaches toward achieving the same end. On the other hand, it is felt that the results presented here provide a reasonable characterization of an AOTV subject to the guidelines used and any great leaps in technological development.

#### AEROASSIST BACKGROUND

Several concepts have been proposed for NASA's Orbital Transfer Vehicle (OTV), and performance trade studies have been performed to compare these concepts. This background section will address those trade studies that were accomplished to establish the rationale for using aerobraking rather than propulsive braking as well as why the integrated structural concept was proposed for this study. The first study was a comparison of the ratio of initial mass in LEO to the payload mass carried to GEO. Since the cost of each unit of mass into LEO is fixed at \$2860 per kilogram (\$1300 per pound) at current (1984) Shuttle delivery rates, this mass ratio gives a

direct cost indicator for each proposed configuration. The higher the mass ratio (defined as  $W_{LEO}/W_{GEO}$ ), the higher the cost for delivery to GEO.

These mass ratios can be determined analytically as a function of the stage propellant mass fraction  $\lambda = W_p/(W_s + W_p)$ . This independent parameter,

mass fraction, was chosen because historical design data is available that show, to a first order approximation, that the dry weight of an orbit transfer stage is proportional to the full propellant capacity of the stage or

$$W_s = \frac{(1 - \lambda)}{\lambda} W_p$$

where

$\lambda$  = mass fraction

$W_p$  = full propellant mass capacity

$W_s$  = stage dry mass

The aerobraked stage can be characterized in much the same way for convenience and comparison purposes. The scaling law chosen for the aerobraked stage is

$$W_{SAB} = \frac{W_{SAP}}{1 - \lambda_B} \quad \text{and} \quad \lambda_B = \frac{W_{AB}}{W_{SAP} + W_{AB}}$$

where

$W_{SAB}$  = aerobraked stage mass

$W_{SAP}$  = mass of an all propulsive stage with equal propellant capacity as the aerobraked stage

$W_{AB}$  = weight penalty for aerodynamic and TPS surfaces

$\lambda_B$  = aerobrake weight penalty fraction

Then, with the above relationships, the rocket equation

$$\Delta V = g_0 I_{sp} \ln \frac{W_i}{W_f}$$

where

$\Delta V$  = velocity change

$g_0$  = units conversion constant  $32.2 \text{ lb}_m\text{-ft}/(\text{lb}_f\text{-sec}^2)$  in U.S. Engineering System

$I_{sp}$  = specific impulse of the rocket

$W_i$  = weight at start of burn

$W_f$  = weight at end of burn

will allow solution of the functional relationships needed for the weight ratio  $W_{LEO}/W_{GEO}$ . These solutions are

$$W_{LEO}/W_{GEO} = \frac{\lambda^{-1} + e^{-(a_1 + a_2)}}{\lambda^{-1} + e^{-2(a_1 + a_2)}} \quad \text{for the all propulsive stage}$$

and

$$W_{LEO}/W_{GEO} = \frac{\lambda^{-1} + e^{-a_2}}{\lambda^{-1} + e^{-(a_1 + 2a_2)}} \quad \text{for the aerobraked stage}$$

where  $W_{GEO}$  is the mass of payload delivered to GEO,  $W_{LEO}$  is total departure mass, and

$$a_1 = \frac{\Delta V_1}{I_{sp} g_0} \quad a_2 = \frac{\Delta V_2}{I_{sp} g_0} \quad a_3 = \frac{\Delta V_3}{I_{sp} g_0} \quad \text{where}$$

$\Delta V_1 = 2440 \text{ m/sec}$  (8000 ft/sec), GEO transfer orbit insertion

$\Delta V_2 = 1830 \text{ m/sec}$  (6000 ft/sec), GEO circularization

$\Delta V_3 = 90 \text{ m/sec}$  (300 ft/sec), required velocity change necessary to circularize the vehicle's orbit after the aerobraking maneuver

Figure 1 shows the mass ratio for both an aerobraked stage and an all propulsive stage (with  $I_{sp} = 4510 \text{ m/s}$  or  $460 \text{ lb}_f\text{-sec}/\text{lb}_m$ ) plotted as a func-

tion of stage mass fraction  $\lambda$ . The asymptotes 0.7411 and 0.8492 are the stage mass fractions at which the stage has zero delivery capability to GEO. First, note that for a given mass fraction, the aerobraked stage substantially outperforms the all propulsive stage. At a mass fraction of 0.86 (equivalent to a Centaur vehicle) the mass ratio for an aerobraked stage is 4.5, whereas that for a propulsive stage is 22. However, this is an invalid comparison since an aerobraked stage will be heavier than an all propulsive stage because of the mass required for the aerobrake and thermal protection systems.

Prior to the design concept described in this report, the aerobraded vehicles proposed to the agency were more like all propulsive stages with an aerobrake subsystem "bolted-on", much like an afterthought. The straight lines connecting the two exponential curves actually link the design points for the two different stages with the mass ratio of the aerobrake subsystems indicated on the lines. This ratio is computed as a fraction of the total stage dry mass. For example, an all propulsive stage of mass fraction 0.86 with "bolted-on" aerobrake subsystems that weigh as much as 40 percent of the total vehicle dry mass, will equate to the aerobraded stage joined by the line labeled " $\lambda_B = 0.4$ ." Note that for the case discussed

the 40 percent aerobrake is not very efficient. A 30 percent aerobrake is more efficient, but not a windfall benefit as mass fraction increases. Another way to measure the benefit of the aerobrake is shown in figure 2 where the increase in payload to GEO for an aerobraded stage is plotted as a function of the brake mass ratio and the mass fraction of the all propulsive stage to which it is "bolted." This functional relationship is determined in much the same manner as the weight ratios in figure 1. The aerobraded OTV's weight penalty is defined differently to facilitate the calculation. However, the concept of aerosurface penalty is still similar.

Now

$$\lambda_{AB} = \frac{W_{SAB} - W_{SAP}}{W_{SAB}}$$

where

$$\lambda_{AB} = \text{weight penalty factor}$$

Assuming that the two competing OTV's have the same propellant capacity, use the rocket equation to yield

$$\frac{\Delta W_{GEO}}{W_{GEOAP}} = \frac{[e^{2(a_1+a_2)} - 1] - \frac{e^{a_1+2a_2+a_3} - 1}{1 - \lambda_{AB}}}{\frac{\lambda_{AP}}{1 - \lambda_{AP}} - \frac{e^{2(a_1+a_2)} - 1}{e^{a_1+2a_2+a_3} - 1}}$$

Here  $W_{GEOAP}$  is the GEO delivery capability of the all propulsive stage,

$\Delta W_{GEO}$  is the difference between the delivery capability of the aerobraded stage and the all propulsive stage, and  $\lambda_{AP}$  is the propellant mass fraction of the all-propulsive stage.

Again, aerobrakes that are 30 to 40 percent of total dry mass do not accrue much in increased delivery capability. However, previous OTV design studies from aerospace contractors show aerobrake masses to be in this range. Therefore, one must conclude that if aerobraded stages cannot be constructed in a more efficient manner, then they are probably not worth the

additional complexity in vehicle design or operation. It was this conclusion that prompted consideration of possible concepts of integrated structures wherein structural support of tanks, engines, thermal protection systems, and other subsystems is shared in order to reduce aerobrake weight penalty. The concept described herein achieves that goal.

#### VEHICLE CONCEPT AND GROUND RULES

The AOTV concept is an ellipsoidally blunted, raked-off elliptical cone and is an extension of the concept evaluated from an aerothermal and thermal protection viewpoint in reference 1.

Many concepts of orbital transfer vehicles have been considered over the last few years (refs. 2-7). All-propulsive vehicles use rocket thrust to produce the necessary velocity decrease to achieve a LEO after return from GEO. Aeroassisted vehicles use the drag of the atmosphere to accomplish the majority of the velocity decrease. There have been a number of concepts investigated in the past including the ballute; the fixed drag brake offering no lift; lifting brakes, including both high and low lift concepts; and aeromaneuvering vehicles that have high lift. Most of these concepts are envisioned as having an aerobrake device attached to an existing cylindrical propulsion module that would fit in the payload bay of the Space Shuttle Orbiter. This study considers a concept that departs from that requirement in that it is an integrated system that would be assembled in space. The aerobrake structure and the components of the propulsion and other systems are integrated to obtain structural efficiency and therefore smaller mass.

The AOTV concept assumes certain ground rules and features. The vehicle is designed to be space-based; that is, it may be assembled in orbit at a space station and is not required to be capable of returning to Earth in the Shuttle payload bay. Components will be brought to LEO from the ground in the Shuttle payload bay for assembly. The vehicle is propelled by liquid hydrogen/oxygen engines. The total useable propellant mass assumed for this study is 38 000 kg (84 000 lb), which defines the basic capability of the vehicle. This particular amount of propellant was chosen for comparison with other concepts studied in the past having the same total propellant.

The present concept assumes the delivery of payloads to GEO and the return of payloads including a 6800 kg (15 000 lb) manned capsule to LEO. The vehicle must be reusable, reliable and require a minimum of maintenance or refurbishment. Operationally, it is envisioned that the vehicle will make a plane change from a 28.5° inclination orbit to an equatorial orbit and back by propulsive impulse. The majority of the velocity decrease in returning from GEO to LEO will be accomplished by aerobraking. The need for lift is relegated to control of the vehicle in the atmosphere and not for significant plane changes.

Because of the possibility of a manned return, a single atmospheric pass is baselined

An aluminum structure is baselined, although composite materials are known to be more mass-effective and, therefore, may be preferable in the ultimate vehicle.

### GEOMETRICAL CONCEPT DESCRIPTION

The geometrical shape of the aerobrake structure was chosen to be a blunted wide angle cone that serves as part of the structure of the stage (figs. 3 and 4). The particular cone is an elliptical cone ( $\theta=60^\circ$  in the x-y plane) raked-off at an angle of  $73^\circ$ . The wide-angle cone was selected because it has a flatter shape for surface area efficiency and it provides lower stagnation point heating than sharper cones. The base of the cone (in the rake plane) is circular, thus defining, along with the rake angle and cone angle, the cone ellipticity. A circular base is not required, but is considered here for packaging reasons.

An ellipsoidal bluntness was chosen which is tangent to the elliptic cone in a planar intersection perpendicular to the cone axis. A bluntness ellipticity (major-to-minor axis ratio) of 2.0 was chosen because it has a rather uniform heat flux distribution and relatively low stagnation point heat flux (ref. 7).

### AERODYNAMICS

The Newtonian lift-to-drag (L/D) ratio is determined by the rake angle with L/D approximately equal to  $\cot \delta$  (ref. 8). In the present study the de-

sired L/D of 0.3 requires a rake angle of  $73^\circ$  and appears to be sufficient for control of the vehicle during atmospheric flight (refs. 9 and 10).

This configuration trims at an angle of attack of zero with respect to the cone axis, thus placing the stagnation point on the maximum radius of curvature of the ellipsoid.

Newtonian aerodynamic characteristics of the concept are shown in figure 5. At an angle of attack  $\alpha = 0$  the lift and drag coefficients are 0.45 and 1.53 respectively, resulting in an L/D of 0.296. The change in pitching moment about the midpoint of the rake plane is  $C_{m\alpha} = 0.0031$  per degree.

The change in yawing moment about the same point due to sideslip angle is  $C_{n\beta} = 0.0033$  per degree. These coefficients represent a statically stable vehicle.

### VEHICLE CONCEPT

The layout of the vehicle was arrived at by balancing various requirements and considerations. One ground rule for the study was that the vehicle be transportable in sections in the Orbiter payload bay. This established the maximum propellant tank diameter. A useable propellant capacity of 38 000 kg (84 000 lb) was assumed which defined the total propellant tank volume. For a given volume, a minimum tank mass is achieved by using fewer, but larger tanks. However, to reduce boiloff during an extended dwell time at

GEO, one full liquid hydrogen fuel tank is dedicated to the descent propulsive maneuvers. This avoids having large partially filled tanks at GEO in which the surface area to volume ratio is not minimized. Heat transfer through the large surface area would lead to excessive loss of hydrogen due to boiloff. Boiloff is very costly due to the high price of transportation to LEO from Earth. This arrangement is also convenient from a packaging standpoint (fig. 6). Since boiloff is not as great a problem for liquid oxygen, only one liquid oxygen tank is included in the design, and it is used for both ascent and descent propulsion.

Two upgraded RL-10 engines having a thrust of approximately 67 000 N (15 000 lb) each are included in the design. Two engines allow for a failure of a single engine without losing the vehicle.

The payload shown in fig. 6 as a cylinder is located as it would be for descent. It is thus protected from heating during aerobraking. A payload that is to be delivered only to GEO may be attached to the vehicle at the opposite side of the aerobrake from the engines, thus allowing for additional flexibility in payload configuration. In the present study the payload is assumed to be a 6800 kg (15 000 lb) manned capsule that is brought back to LEO, although it is seen that a greater payload return capability is possible from performance and aeroheating standpoints.

#### PROPULSION

A propulsion system on an OTV utilizing an aerobrake must be integrated with two other major elements, the aerobrake and the payload, rather than just the payload as on an OTV without an aerobrake. Three different engine firing arrangements are possible: side-firing, firing through the aerobrake, and firing away from the aerobrake. The last firing arrangement would require the engines and propellant tanks to be placed around the periphery of a centrally located payload. If the payload is fairly long, exhaust from the engines will impinge upon the payload. Firing through the aerobrake, like a conventional stage, would place the payload atop the propulsion system with the aerobrake added below extendable nozzle engines. The required doors in the aerobrake would add complexity and be unsafe for manned missions, allowing a fatal single point failure. Therefore, side firing would be the preferred arrangement for an aerobraked OTV.

To limit the size of the aerobrake, the propulsion system must be sandwiched between the payload on one side and the aerobrake on the other. With different payload masses and propellant quantities, the center of gravity of the vehicle will shift laterally with respect to the engine firing direction. A conventional stage would see little of this lateral shift in the center of gravity. Therefore, greater engine gimbaling capability will be required to maintain the thrust through the center of gravity. Placement of the engines close to the line of center of gravity movement and placing the oxygen tank and payload as far away from the engines as possible (e.g. opposite side of aerobrake) may be required to minimize the gimbaling. Also, the distance between the payload and the aerobrake should only accommodate one tank, even though stacking the tanks will result in a smaller aerobrake. In addition, the variable thrust direction may result

in an increase in propellant residuals because the propellant settles at different angles with respect to the tank outlet. If future analysis determines that residuals need to be reduced, conical tank sections at the outlet or acquisition screens may be required.

The placement of the propellant tanks on the aerobrake surface will determine the size of the aerobrake. A conventional tandem arrangement of tanks with a single tank for each propellant would provide the minimum tank weight and propellant boiloff while covering the minimum aerobrake surface. However, the total area required for this arrangement with an aerobraked vehicle having an elliptical plan form would be greater than evenly distributing the tanks on an aerobraked vehicle having a circular plan form. It was primarily this packaging problem that drove the design for the aerobrake configuration to a raked elliptical cone, because the projection of the shape into the rake plane was a circle whereas the similar projection of a circular cone is an ellipse. Thus, the selected configuration appears circular when viewed from the top, and this configuration offered better packaging for the propulsion tankage. A single cylindrical oxygen tank and two cylindrical hydrogen tanks allowed a compact, even distribution of tanks. The addition of a spherical hydrogen tank filled the gap between the main tankage and the engines while allowing the boiloff to be minimized for the hydrogen required for descent from GEO. With the spherical descent hydrogen tank, the boiloff would be minimized because the surface area is at an absolute minimum. The added surface area in the two cylindrical hydrogen tanks does not greatly affect boiloff because of the limited time required to perform the ascent portion of the mission.

Two RL-10 IIB engines were chosen for this concept. This upgraded version of the engines used on the Centaur has a specific impulse typical of the more advanced expander cycle engines; and the extendable nozzle is required to prevent impingement of the exhaust on the aerobrake and also allows the nozzle to be out of the high enthalpy entry flow. A minimum of two engines are required for safety during manned missions, so that one engine can always backup a failed engine.

#### VEHICLE STRUCTURE CONCEPT

To obtain the objective of a minimum mass structure for the total system the integrated design was chosen as shown in figure 6. The propellant tanks are supported by trunnions connected to web bulkheads which also form part of the main thrust structure. Transverse bulkheads provide rigidity normal to the thrust direction. The aerobrake structure is a lightweight closed isogrid with a skin.

The engines are tied to the thrust structure with struts and the payload is attached to the structure such that the loads are distributed uniformly through four hard points.

Several gauges of structural materials were used in the design analysis. Materials of various dimensions were used in different locations according to load requirements. A schematic of the structural design is given in figures 7 and 8.

## STRUCTURAL MASS ESTIMATE

A Nastran model was made of the 12-meter (40-ft) diameter, blunted, raked-off conical AOTV design in order to make a preliminary mass estimate. The heat shield was modeled using shell elements representing two different patterns of closed isogrids. The engine and propellant tank mounting struts were modeled using three sizes of rod elements. The bulkheads were modeled using simple plate elements. The propellant tanks were modeled as concentrated masses and rigid bars. Although the actual mass is less, the

thermal protection system was modeled as being  $6.3 \text{ kg/m}^2$  ( $1.3 \text{ lb/ft}^2$ ) of nonstructural mass applied to the heat shield shell elements. All other components of the vehicle were accounted for with concentrated masses.

Three load cases were examined. Cases 1 and 3 were aerobraking descents at 3 g with no payload and with 6800 kg (15 000 lb) of payload, respectively. Load case 2 was a propulsive ascent at 2 g with a 28 000 lb payload and a full propellant load of 39 000 kg (86 000 lb). On an actual vehicle, powered flight at 2 g acceleration would occur only when the propellants were nearly depleted. Therefore, this load case was extremely conservative.

A safety factor of 2 was used throughout the analysis. All elements had positive margins of safety under all load cases. No buckling analysis was performed and the bulkheads used on an actual vehicle would require stiffeners and might be replaced by open isogrid panels or truss assemblies. This is not expected to change the mass estimate significantly.

Aluminum 7075 properties were used for all structural components. Tank masses were estimated using aluminum 2219 properties. The structural mass could be cut roughly in half with the use of composite materials, at the price of increased manufacturing costs, additional design work, and possible service life limitations, depending on the material chosen.

The total estimated structure mass is 681 kg (1499 lb) composed of 375 kg (825 lb) for the heat shield structure, 206 kg (453 lb) for the bulkheads, and 100 kg (221 lb) for the struts. The total tank mass estimate is 1303 kg (2869 lb) which includes thermal insulation, micrometeoroid protection, baffles, and plumbing.

## AEROBRAKING TRAJECTORY

Preliminary trajectory simulation using the 1962 standard atmosphere produced the trajectory plots shown in figures 9-12. Entry conditions were 10 311 m/sec (33 829 ft/s) velocity and  $-4.52^\circ$  flight path angle to simulate return from GEO for an entry mass of 13 200 kg (29 000 lb) and  $m/C_D A =$

$73.8 \text{ kg/m}^2$  ( $15.1 \text{ lb/ft}^2$ ). The guidance scheme (ref. 9) computes reference dynamic pressure and altitude rate to target the vehicle to a 370 km (200 nmi) apogee after atmospheric exit. The minimum altitude reached was 76 km (250 000 ft), producing maximum dynamic pressure and maximum g-load of 1500

$\text{N/m}^2$  (32 psf) and 2.2 g respectively. The desired inclination of  $28.5^\circ$  was achieved with four bank reversals.

Preliminary analysis of vehicle performance in response to entry, aerodynamic, and atmospheric uncertainties shows adequate controllability with a  $5^{\circ}\text{s}^{-2}$  roll acceleration and a  $17.5^{\circ}\text{s}^{-1}$  maximum roll rate (ref. 11).

### AERODYNAMIC HEATING ESTIMATES

The heat flux estimate follows that presented in reference 1. Heat flux to the aerobrake windward surface is estimated using the trajectory correlation

$$q \sqrt{R_N} = 7.3 \left( \frac{m}{C_D A} \right)^{0.467} \left( \frac{L}{D} \right)^{0.242} (\text{W/cm}^2) \text{ m}^{1/2} \quad (1)$$

where

$q$  = heat flux

$R_N$  = nose radius at stagnation point

$m$  = mass of vehicle at entry

$C_D$  = drag coefficient

$A$  = reference area

The heat flux used to obtain equation 1 is based on the engineering correlation for the heat flux to the stagnation point of a reference sphere

$$q \sqrt{R_N} = 18\,300 p_{\infty}^{1/2} (V_{\infty}/10^4)^{3.05} (\text{W/cm}^2) \text{ m}^{1/2} \quad (2)$$

where

$p_{\infty}$  = free stream density

$V_{\infty}$  = free stream velocity

Using this correlation (eq. 1) results in a small difference from the value calculated from (eq. 2) when the actual trajectory conditions are used.

Through geometrical considerations the heat flux to the stagnation point could be obtained. Using the above formulas with an aerobrake diameter of 12 m (40 ft) and mass of 13 200 kg (29 000 lb) the peak heat flux was found to be  $26 \text{ W/cm}^2$  ( $23 \text{ Btu/ft}^2\text{-s}$ ) for a fully catalytic surface. Assuming a factor 0.75 to account for finite rate catalysis the estimated peak stagnation point heat flux is about  $19 \text{ W/cm}^2$  ( $17 \text{ Btu/ft}^2\text{-s}$ ). This corresponds to

a temperature of 1430 K ( $2110^{\circ}\text{F}$ ) based on radiation equilibrium. This temperature is well within the capability of the current Space Shuttle tile material used on the lower surface of the Orbiter.

The heat flux to other areas of the aerobrake windward surface is assumed to be no greater than the stagnation point value. Shock layer radiation is

assumed to be small (ref. 12) and is neglected. A representative heat flux distribution for a similar body is shown in figure 13. This distribution is calculated using a 3-D Navier-Stokes numerical solution (ref. 13). The difference between the actual body and the one shown in figure 14 (used for the calculations) is the handling of the skirt. For the calculation the skirt is extended considerably and has a large radius of curvature. This may have the effect of reducing the predicted skirt heat flux below a realistic value.

### THERMAL PROTECTION

The thermal protection system (TPS) envisioned for this study is an extension of Shuttle Orbiter technology. It is believed that there will be improvements in materials and concepts over the next few years, but these potential improvements will be ignored in the present study. The capability of the Shuttle high temperature reusable surface insulation (HRSI) tiles is

quite within the peak heating estimate of  $19 \text{ W/cm}^2$  ( $17 \text{ Btu/ft}^2\text{-s}$ ). The proposed TPS consists of HRSI tiles bonded with room temperature vulcanizing silicone rubber (RTV) to a strain isolation pad which is bonded to the aluminum skin of the aerobrake. As in the Shuttle design, the tile thickness requirement is based on the aluminum skin not exceeding a temperature

of  $450 \text{ K}$  ( $350^\circ\text{F}$ ). This is a somewhat arbitrary requirement for an AOTV. The tile thickness (approximately 12 mm) is based on the stagnation point heat load, and that thickness is assumed to be uniform over the entire aerobrake. Thinner or lighter materials could be used in lower temperature regions of the aerobrake and hence save weight; however, this refinement was not incorporated here. Figure 16 of reference 7 is used in this study to estimate the TPS mass per unit area, which was found to be

$3.2 \text{ g/m}^2$  ( $0.66 \text{ lb/ft}^2$ ) for an effective structure thickness of  $\bar{t} = 0.254 \text{ cm}$  ( $0.1 \text{ in}$ ). For an aerobrake surface area of  $146 \text{ m}^2$  ( $1570 \text{ ft}^2$ ), this results in a total aerobrake TPS mass of  $468 \text{ kg}$  ( $1030 \text{ lb}$ ).

### TOTAL VEHICLE MASS

To obtain a total vehicle mass it was necessary to assume values for various subsystem components. These were estimated on the basis of current state-of-the-art allocations and previous OTV studies.

A summary of the calculated and assumed masses is given in table 1. To obtain the mass at reentry a factor of 1.0242 was applied to the end-of-mission estimated mass. This factor accounts for additional fuel on board at the beginning of the atmospheric phase of the flight, subsequently used for circularization and LEO maneuvering.

It can be seen from the table that the total aerobrake mass, including its thermal protection system, is about 17 percent of the total end-of-mission stage mass excluding the  $6800 \text{ kg}$  ( $15\,000 \text{ lb}$ ) payload. This factor is much smaller than previously estimated for aerobrakes that are attached to an independent or nonintegrated stage and is approximately the same as that estimated for a ballute concept (ref. 5). If one constructed the vehicle

from composite materials such as graphite polyimide or graphite epoxy, the structural mass would be several hundred kilograms lighter and the aero-brake mass fraction would be decreased to about 13 percent. Thus, the concept studied here is highly competitive based on mass considerations.

### PERFORMANCE

Performance estimates for service to and from GEO were made based on the following assumptions:

1. Impulsive burns
2.  $I_{sp} = 4500$  m/sec ( $460$  lb<sub>f</sub>-sec/lb<sub>m</sub>) with 1 percent degradation for start and stop losses
3. Flight performance reserves assumed to be 2 percent of the  $\Delta V$  applied at each burn
4.  $\Delta V$  assumptions:

For GEO missions

GEO transfer	2400 m/s	(8000 ft/s)
Mid-course	15 m/s	(50 ft/s)
GEO circularization	1800 m/s	(6000 ft/s)
LEO transfer	1800 m/s	(6000 ft/s)
Circularization at LEO after aerobraking	91 m/s	(300 ft/s)

For lunar missions

Translunar	3150 m/s (10,350 ft/s)	first stage
Mid-course	66 m/s (180 ft/s)	second stage
Lunar circularization	970 m/s (3190 ft/s)	second stage
Descent	2100 m/s (6890 ft/s)	second stage
Ascent	1920 m/s (6292 ft/s)	second stage
Trans-Earth	947 m/s (3107 ft/s)	second stage
Mid-course	55 m/s (180 ft/s)	second stage
LEO circularization after aerobraking	94 m/s (310 ft/s)	first or second stage

5. Reaction control system propellants = 1 percent of main impulse propellants

6. End-of-mission residuals = 438 kg (964 lb)

Using these assumptions the stage performance is

GEO delivery mass 13 500 kg (29 800 lb)

Round-trip payload mass 7130 kg (15 700 lb)

Mass ratio to GEO 4.334

Lunar surface delivery mass 18 800 kg (41 500 lb)

Round-trip to lunar surface 6800 kg (15 000 lb) with 3860 kg (8500 lb) excess payload mass one-way to surface

Mass ratio to lunar surface 6.1

Figure 15 shows a comparison of this aerobraked stage with a similar all propulsive stage with the same propellant load. The left hand ordinate  $W_{GEO}/W_{GEOAP}$  is a measure of the additional payload delivered to GEO by an

aerobraked stage normalized by the GEO payload capability of the identical all propulsive stage. The abscissa is the additional weight penalty of the aerobraked stage. The plotted curve shows the percentage increase in GEO delivery capability of an aerobraked stage as compared to an all propulsive stage. Note that if the aerobraked stage was 50 percent heavier than the equivalent propulsive stage, there is no performance improvement possible with the aerobraked stage. However, as the weight penalty for the aero surfaces approach zero, the performance improvement approaches a maximum limit of 96 percent. The design in this report, shown to be at the 17 percent point, will yield a 76 percent increase in payload to GEO over the all propulsive stage. Note that the approximation for an all composite structure will yield an 80 percent improvement. Also note that this design is satisfactorily close to the maximum yield of 96 percent. To compare the aerobraked stage with alternative technologies, the right hand ordinate is an indication of the  $I_{sp}$  required of an all propulsive stage to

achieve the same improvement. An  $I_{sp}$  of 5050 m/s (515  $lb_f$ -sec/ $lb_m$ ) would be required in order for an all propulsive stage to make the same GEO delivery; or, looking at the comparison in a different way, the aerobrake is equivalent to a 540 m/s (55  $lb_f$ -sec/ $lb_m$ ) increase in specific impulse. One

final comparison would be the costs saved by this aerobraked stage. This comparison is made by using this aerobraked stage to deliver the 7600 kg (16 800 lb) all-propulsive-limit-payload to GEO, then calculating the reduced launch costs for delivery of propellants to orbit. The aerobraked stage can deliver the 7600 kg (16 800 lb) payload to GEO and save 9676 kg (21 313 lb) of propellants which equates to a \$27.7 million savings in Shuttle launch costs at \$1,300 per pound.

## TECHNOLOGY IMPROVEMENTS

There are several areas of technology in which advances would lead to improved design and performance. Improved engines with greater specific impulse would reduce the total propellant and tank mass. Of course, the engines must be extremely reliable and this places a constraint on their design. Since propellant boiloff reduces that available for propulsion, improved tanks could save propellant and reduce tank size. Reducing the tank size would permit reducing the aerobrake size and thus reduce its mass. The development of composite structural components would reduce the mass of the structure without sacrificing strength or rigidity.

Since the thermal protection system considered in this study is essentially minimum-gauge rigid insulation, the use of a lighter fabric or soft insulation having improved temperature and strength characteristics could reduce the TPS mass.

Improved aerothermodynamic predictions of the heat flux distribution on the aerobrake as well as in the wake or lee side regions of the vehicle will enable tailoring the thermal protection system more accurately and thus reduce conservatism. Improved knowledge of the flow field chemistry and surface catalytic recombination reaction rates will improve heat flux predictions, as will improved numerical flow field computational methods. The latter are particularly important for an AOTV since wind tunnels are limited in their simulation capability at these high altitudes and velocities.

## CONCLUSIONS

This study of an integrated structural design of a lifting brake, aeroassisted orbital transfer vehicle has shown that it is possible to configure a very mass-competitive space-based design. While this rigid design must be assembled in orbit from subassemblies transported in the Space Shuttle payload bay, it has the advantage of not requiring the replacement or repackaging of major components such as an inflatable structure.

The ellipsoidally blunted, raked-off elliptical wide-angle cone has several desirable features, but it should be compared with other lifting brake shapes such as a blunted symmetrical cone with an offset center of gravity. Wind tunnel and computational fluid dynamic analyses will help assess the aerodynamics and aerothermodynamics of each configuration.

For the size of return payload and the tank sizes considered the thermal requirements imposed on thermal protection system are fairly mild and can be satisfied by current technology. This implies that with smaller tanks and return payloads one could reduce the diameter of the aerobrake and significantly reduce its mass without exceeding TPS temperature limits due to excessive aeroheating. This study has assumed that the nonequilibrium shock layer radiative heat flux is very small and is consistent with the calculations of reference 12. If the nonequilibrium radiation were considerably larger as implied by reference 7, then the TPS would be somewhat heavier. With minor improvements in current TPS materials' capability (e.g., a more reflective coating) significant radiative heating can be accommodated.

TABLE 1 - JSC AOTV CONFIGURATION MASS SUMMARY (GEO RETURN)

	Mass (in pounds)	
TPS	1 030	
Heat Shield Structure	825	
Aerobrake subtotal		1 855 (16.7% of stage at EOM)
Bulkheads	453	
Struts	221	
Structure Subtotal		1 499
Stage - payload	585	
Internal insulation	526	
Power and distribution	480	
RCS	449	
Avionics	464	
Tankage	2 869	
Engines (two RL-10)	1 855	
Total dry stage mass	<u>9 757</u>	
Residual & reserve propellant (EOM)	<u>1 337</u>	
End of Mission Mass (Stage)		<u>11 094 lb</u>
Contingency 20%	2 219	
Payload (manned capsule)	15 000	
Total EOM mass	<u>28 313</u>	
Reentry mass 1.024 x EOM mass		<u>28 993 lb</u>
$\frac{m}{C_D A} = 15.1 \text{ lb/ft}^2$		

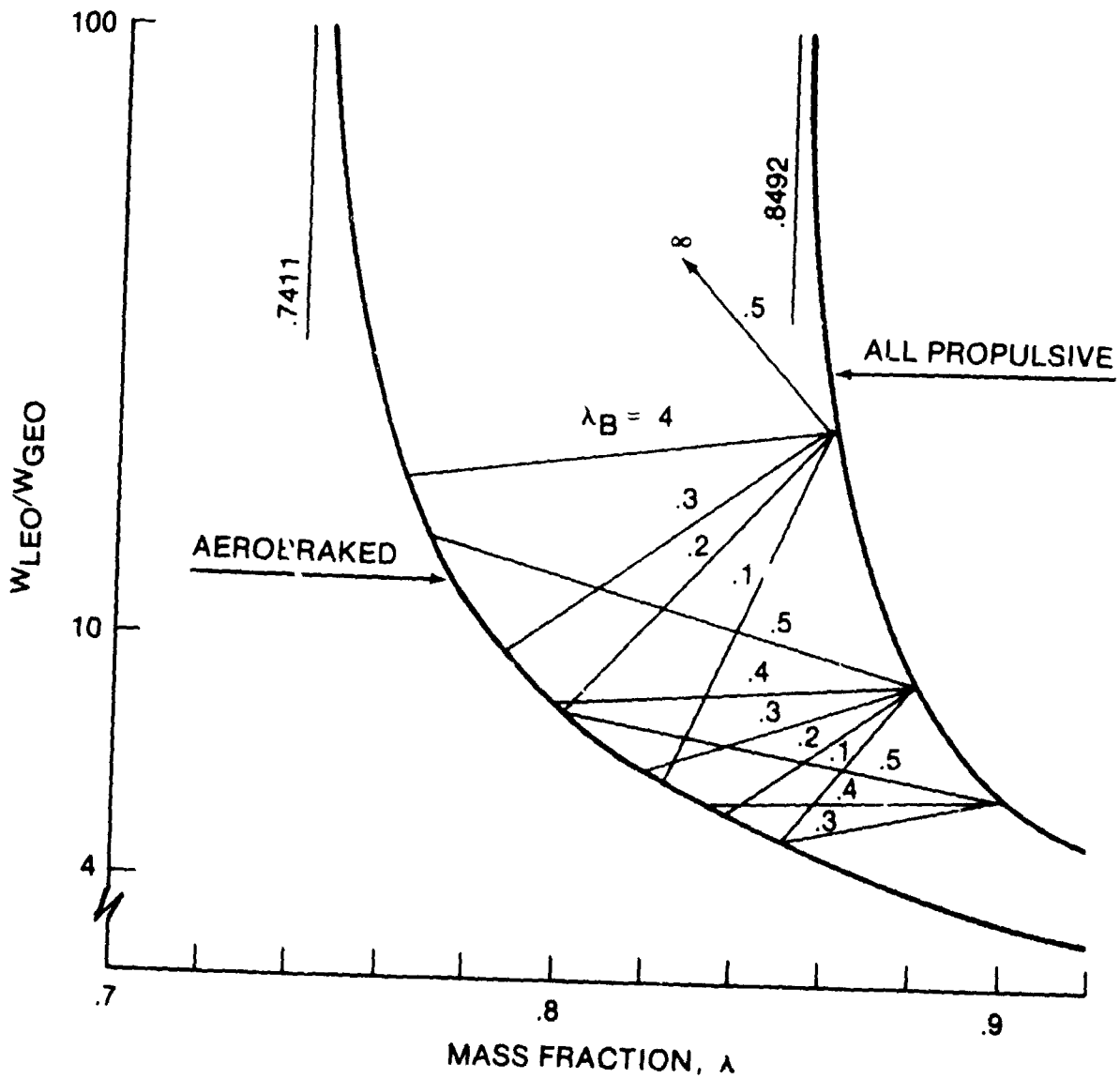


Figure 1. - Payload-to-stage mass ratio of all propulsive and aerobraked stages.

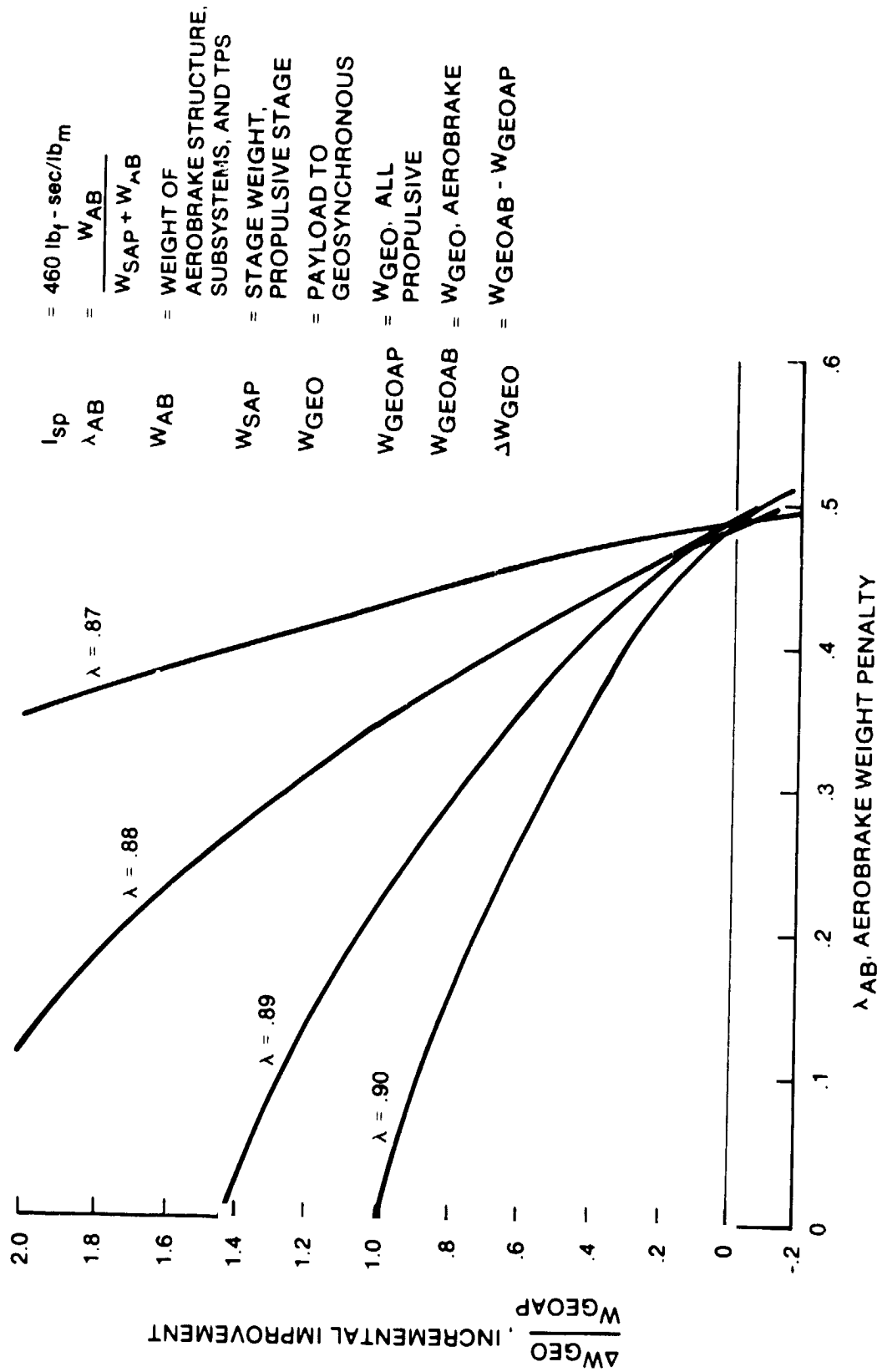


Figure 2.- Improvement in GEO delivery payload compared with aerobrake mass.

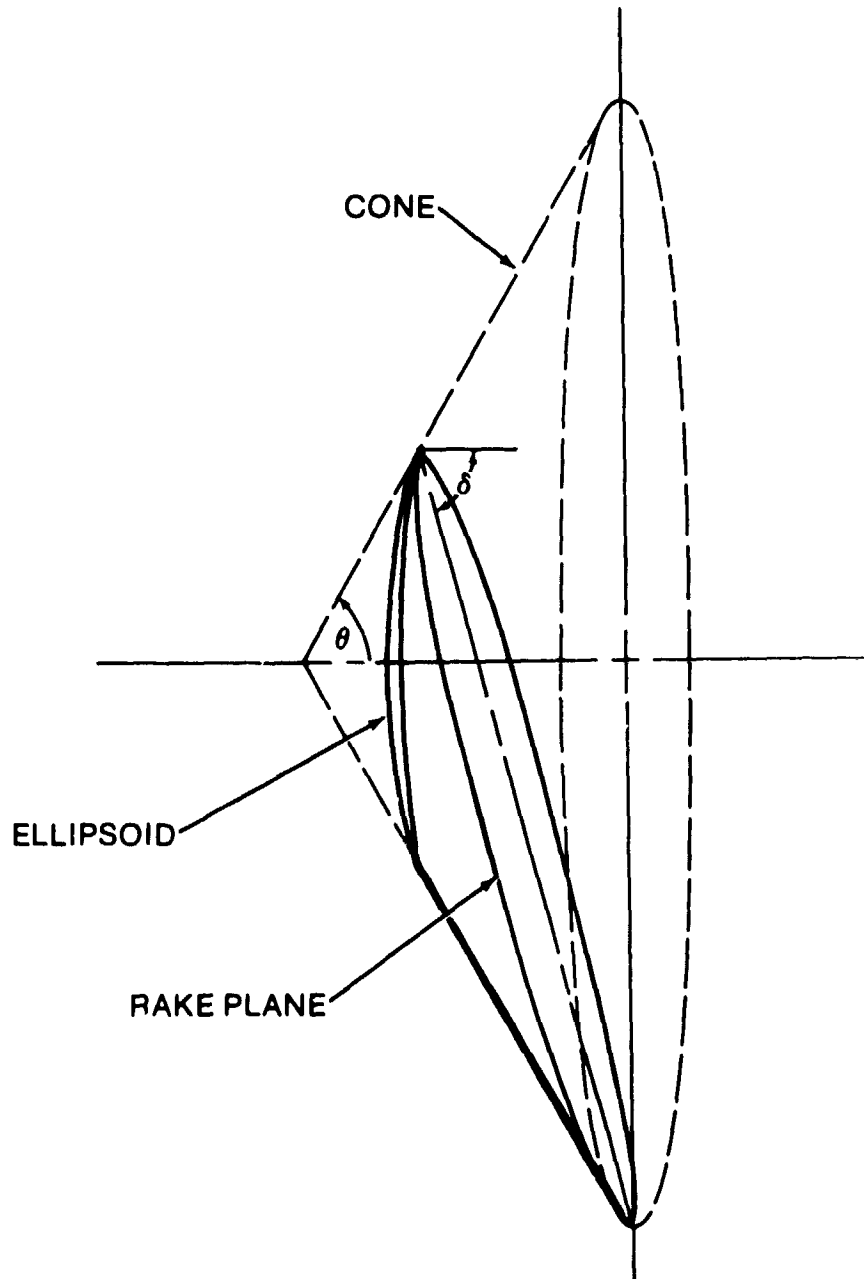


Figure 3. - Geometric construction of blunted, raked-off cone.

ORIGINAL PAGE  
OF POOR QUALITY

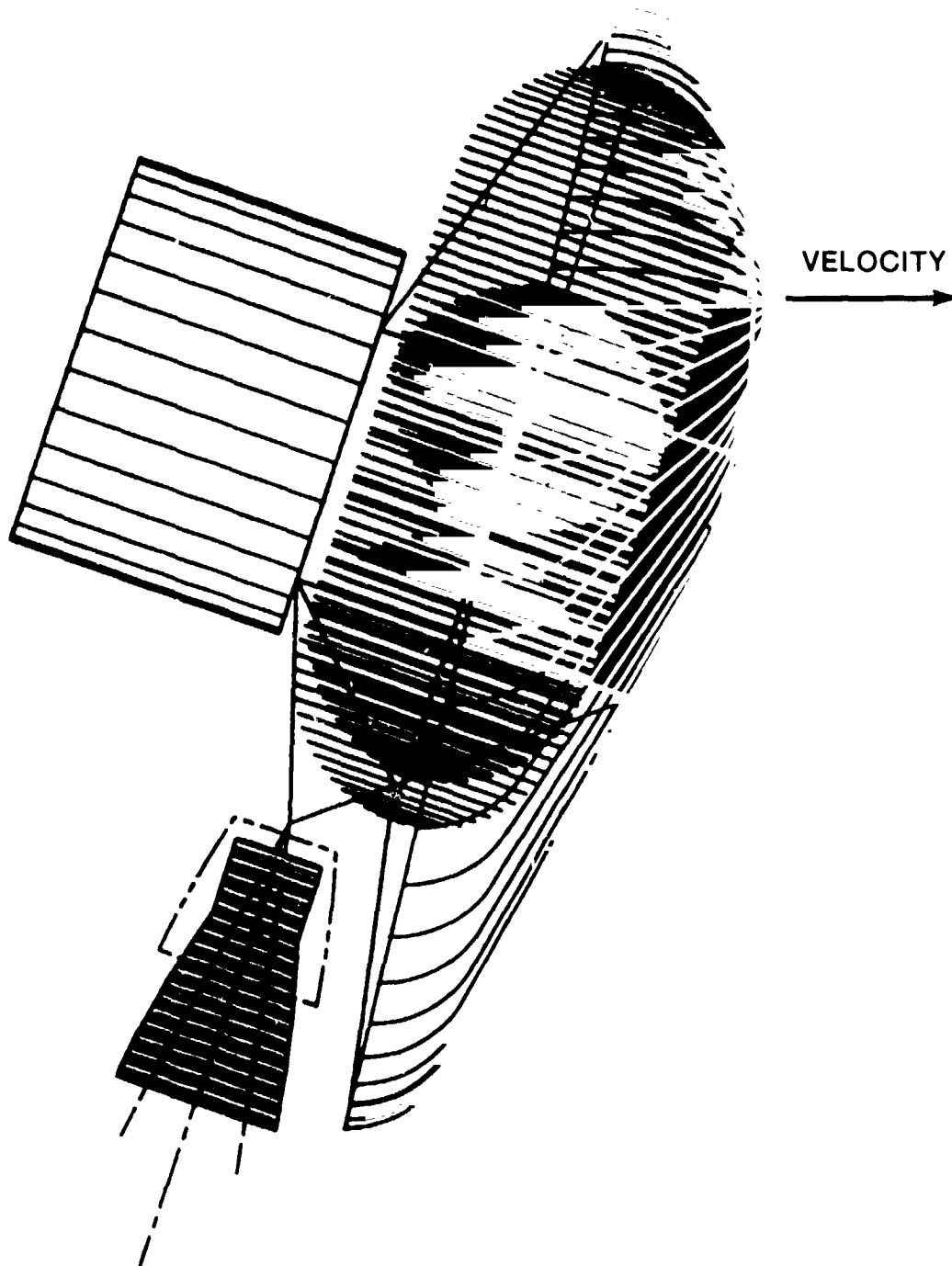


Figure 4. - Integrated AOTV design in aerobraking attitude.

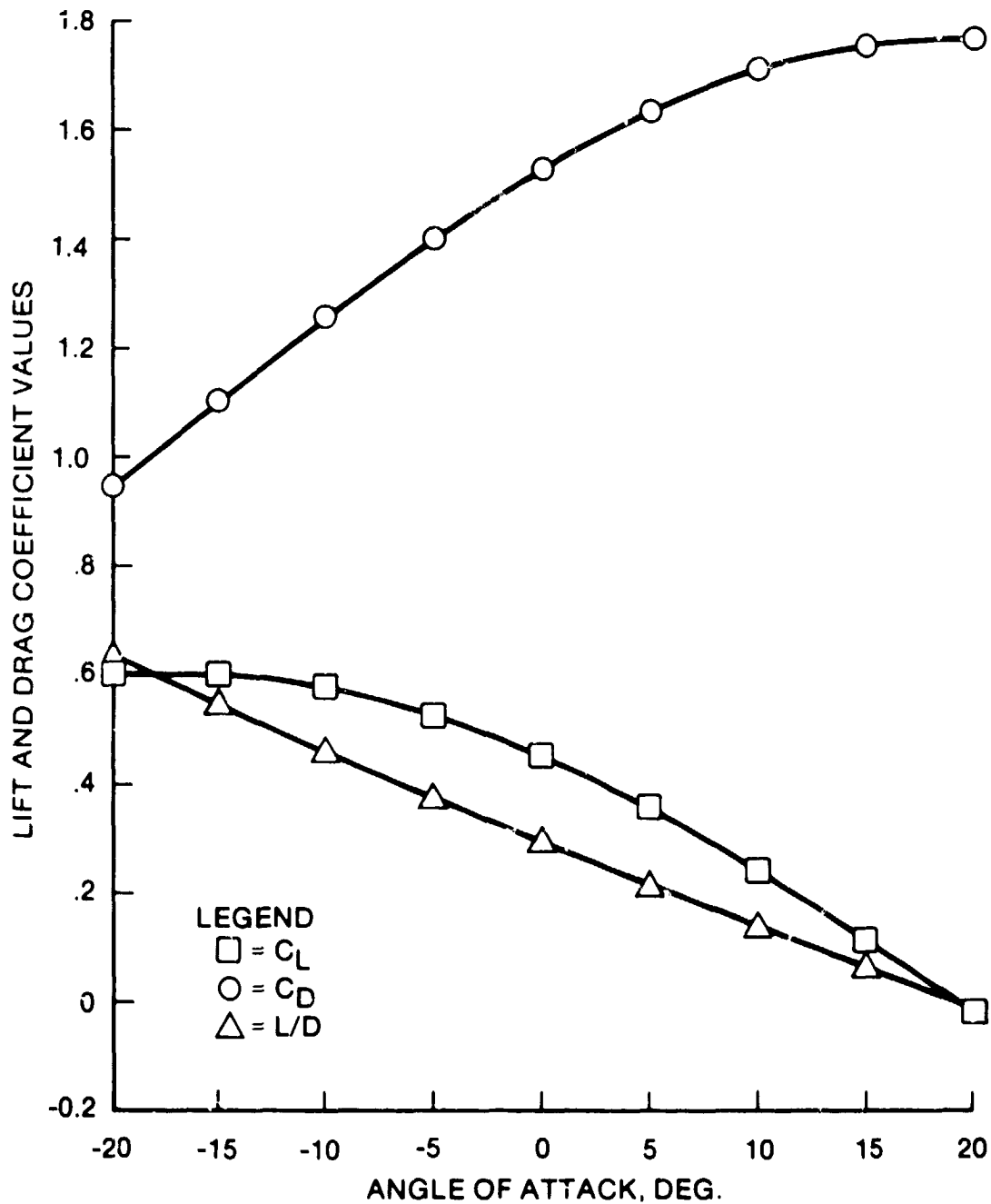


Figure 5. - Newtonian aerodynamic coefficients of blunted, raked-off cone.

ORIGINAL DRAWING  
OF POOR QUALITY.

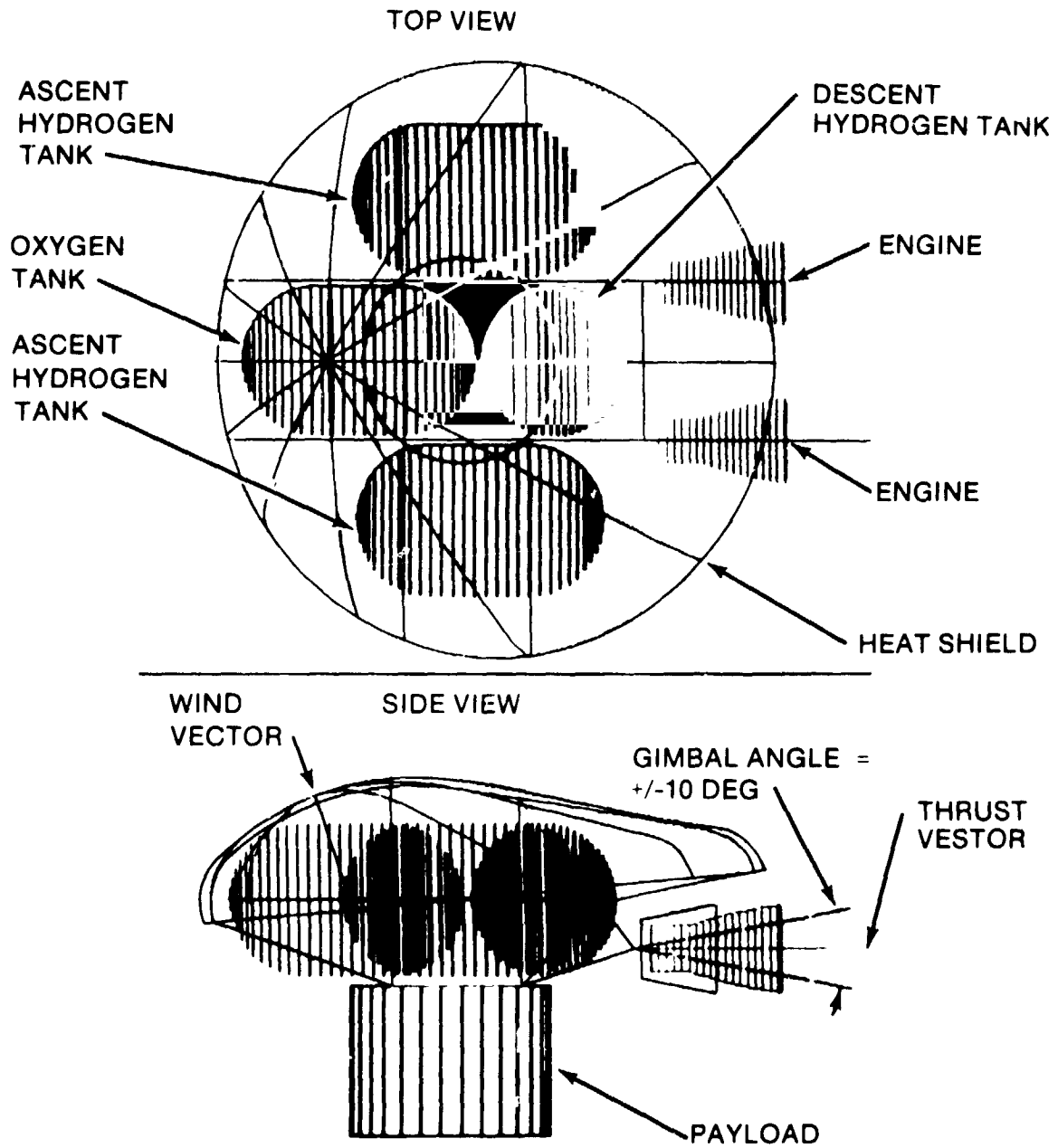


Figure 6. - Integrated AOTV concept with 12-m (40-ft) diameter heat shield.

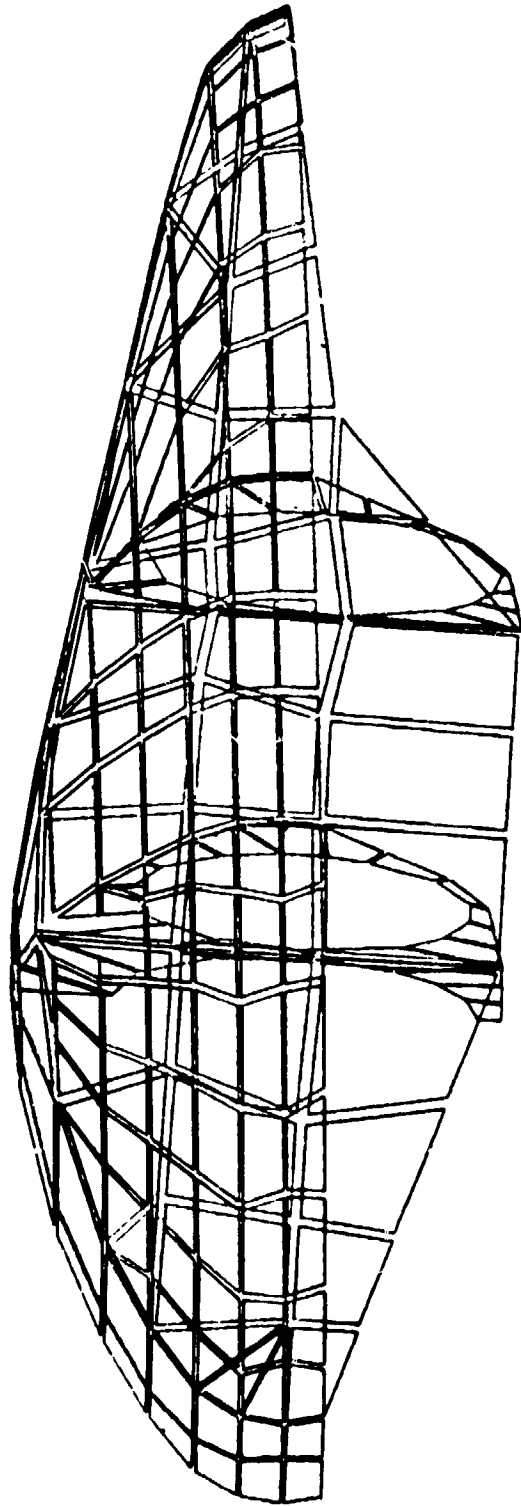
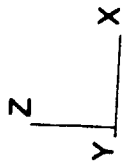


Figure 7. - Side view of half-model AOTV heat shield structure and bulkheads.

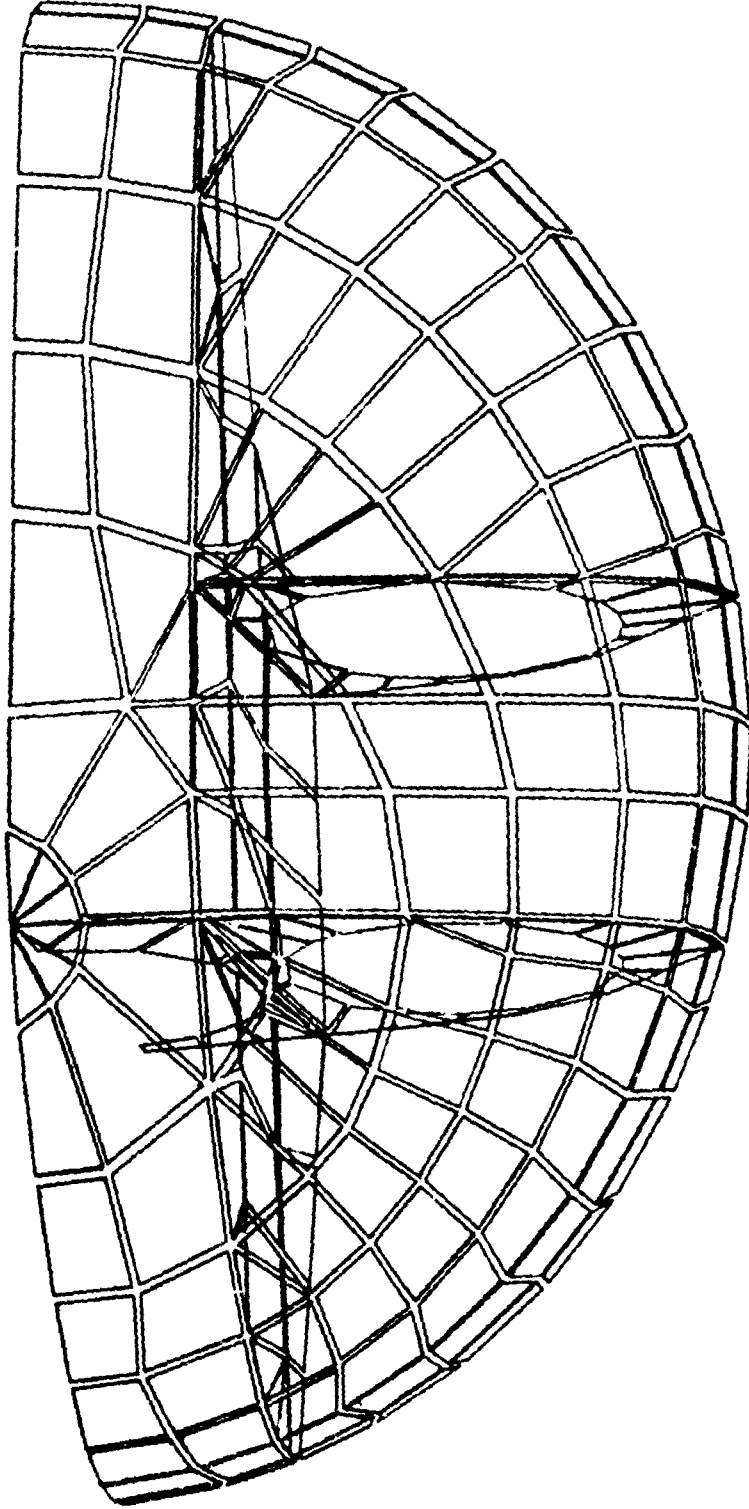
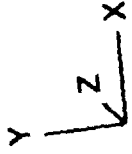


Figure 8. - Front view of half-model of AOTV heat shield structure and bulkheads.

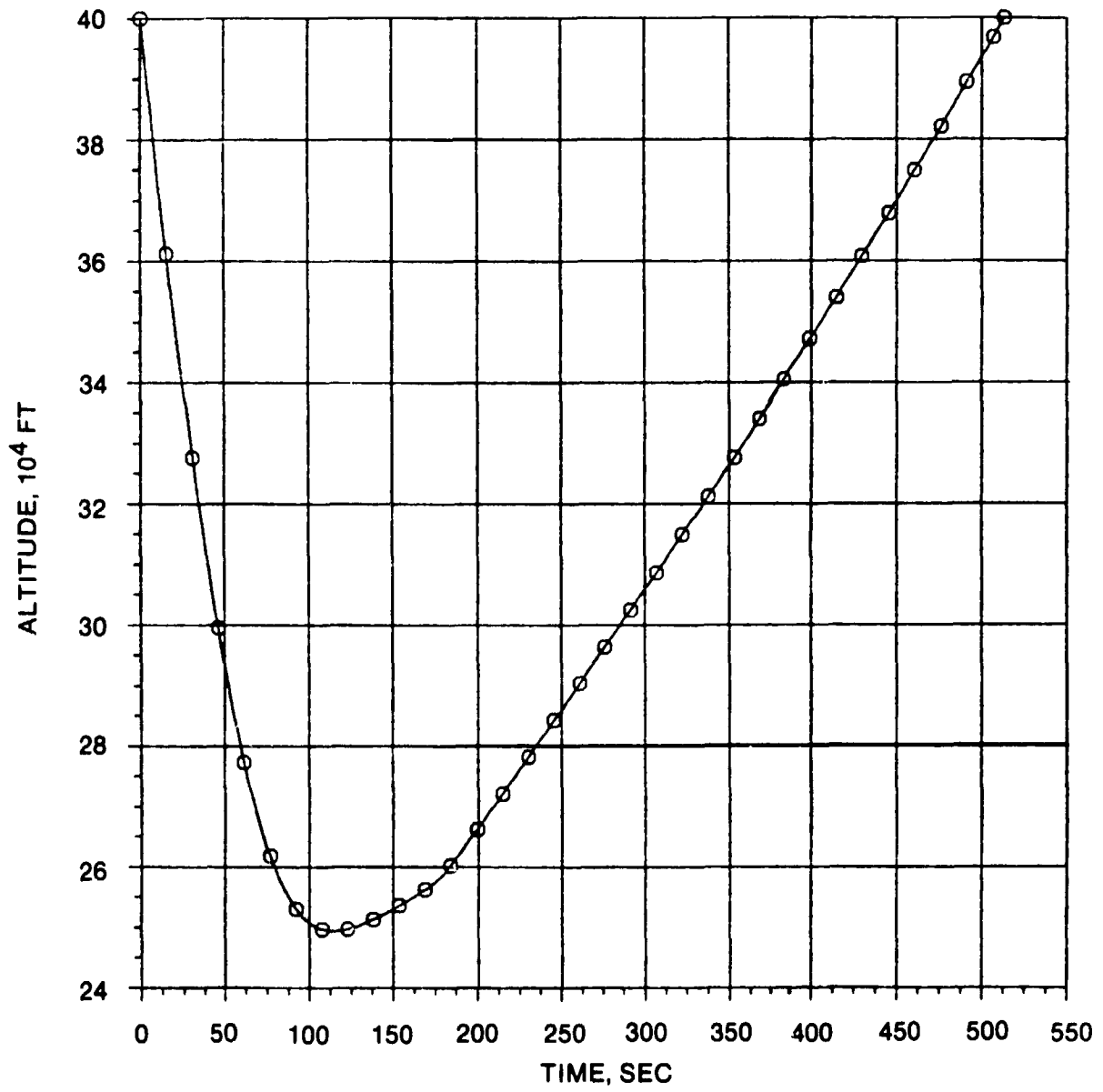


Figure 9. - Altitude time history during AOTV aerobraking.

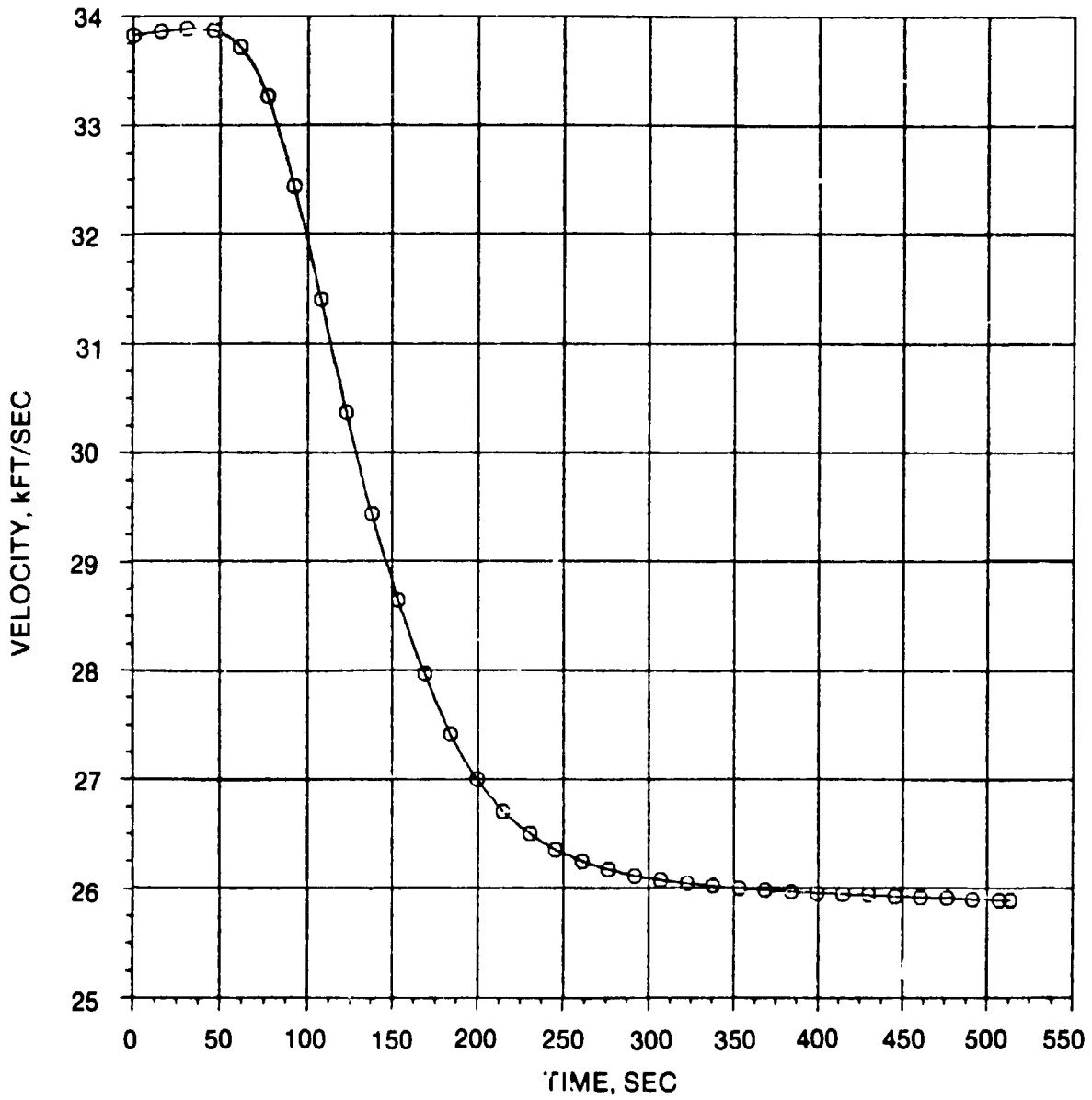
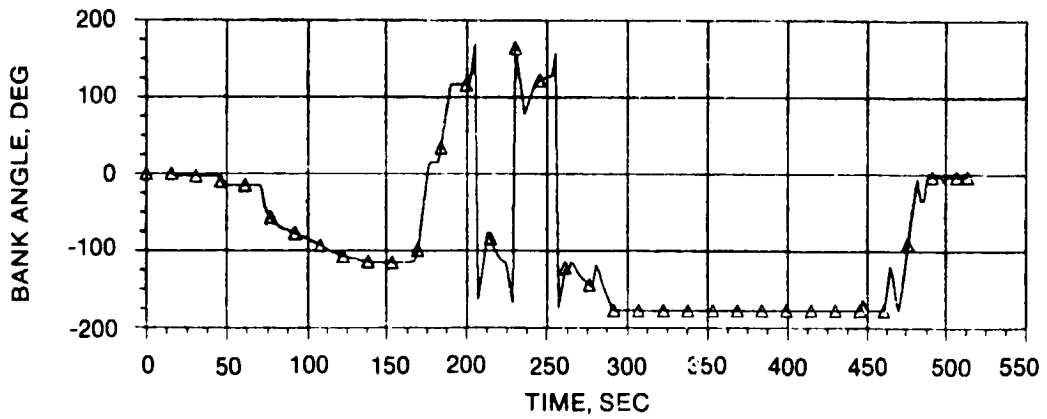
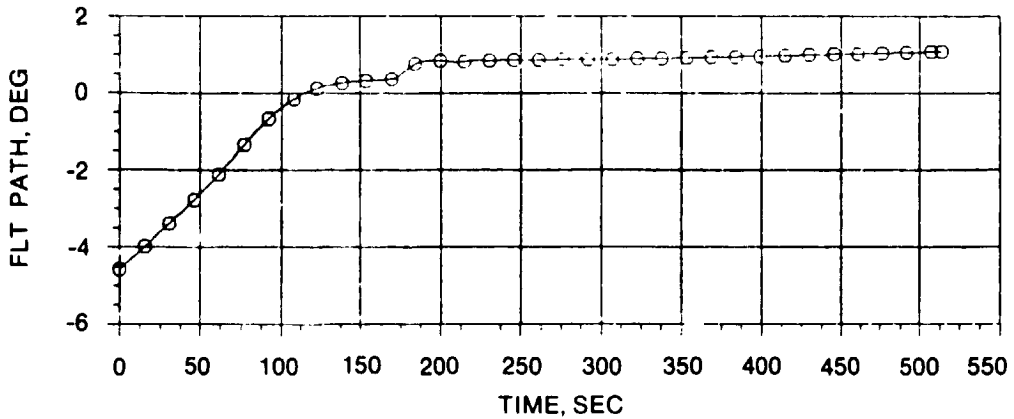


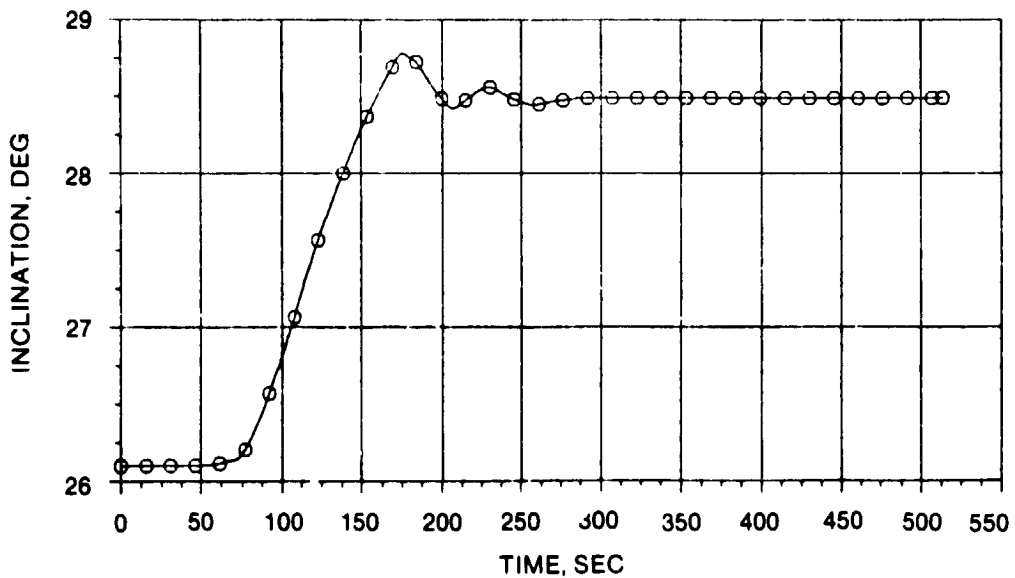
Figure 10. - Velocity time history during AOTV aerobraking.



(a) Bank angle

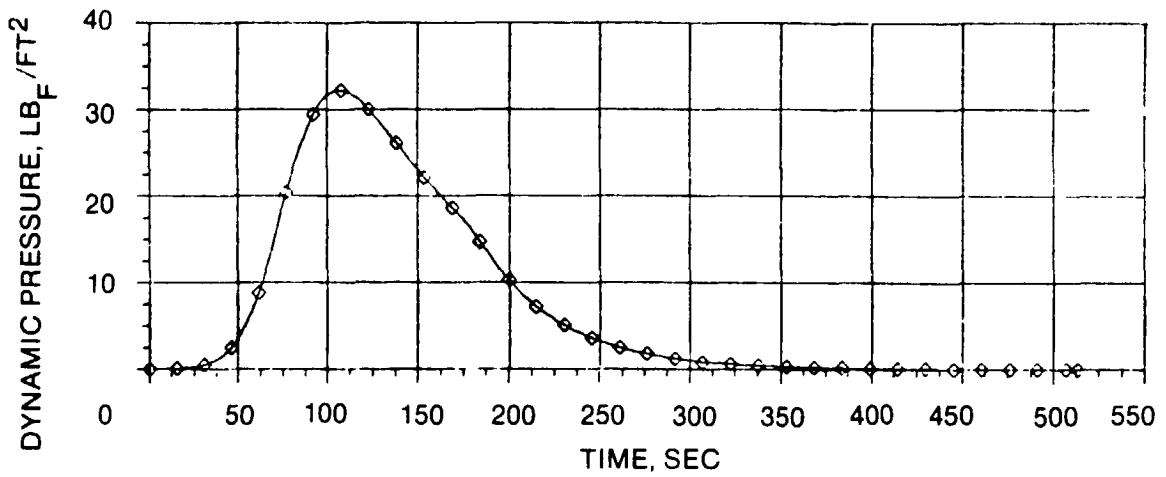


(b) Flight path angle

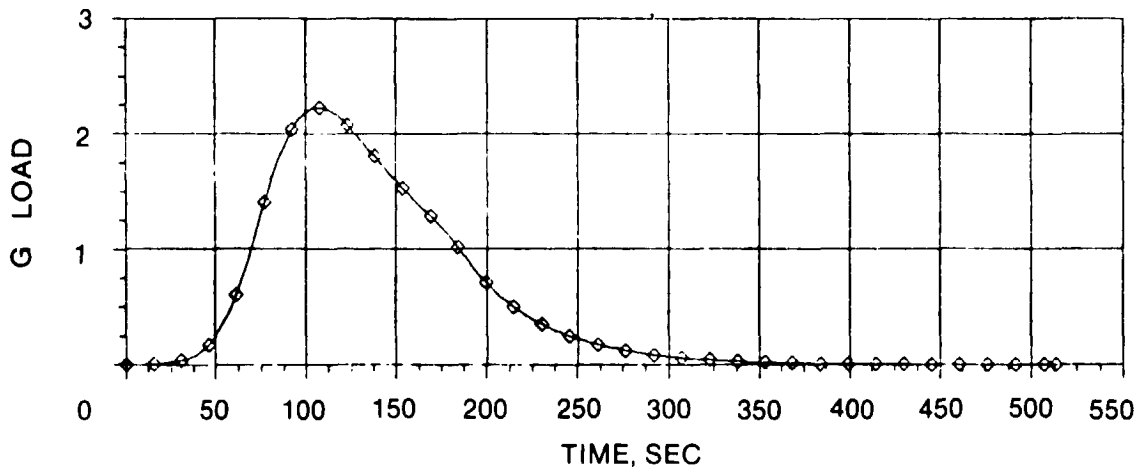


(c) Orbital inclination

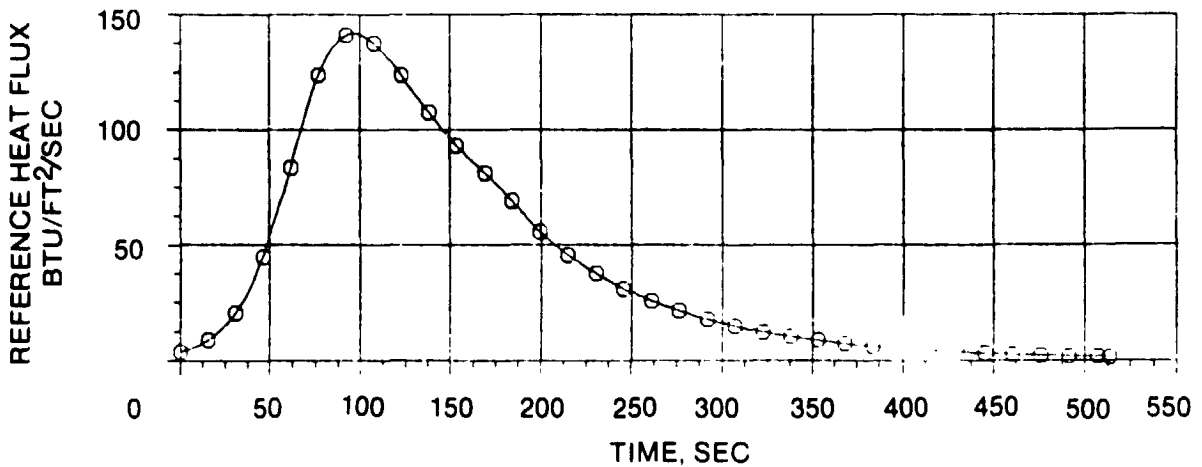
Figure 11. - AOTV atmospheric flight trajectory characteristics.



(a) Dynamic pressure



(b) Atmospheric deceleration



(c) Heat flux to reference 1-FT sphere

Figure 12. - AOTV atmospheric flight environment.

$V_\infty = 9.75 \text{ km/s}$      $M_\infty = 34.8$      $\alpha = 0$     IDEAL GAS     $\rho_\infty = 7.47 \times 10^{-6} \text{ kg/m}^3$      $\delta = 75^\circ$   
 $(32 \text{ kft/s})$      $\theta_{xy} = 60^\circ$      $\epsilon_b = 2$      $R_N = 1.52 \text{ m}$      $(1.45 \text{ slug/ft}^3)$   
 $(5 \text{ ft})$

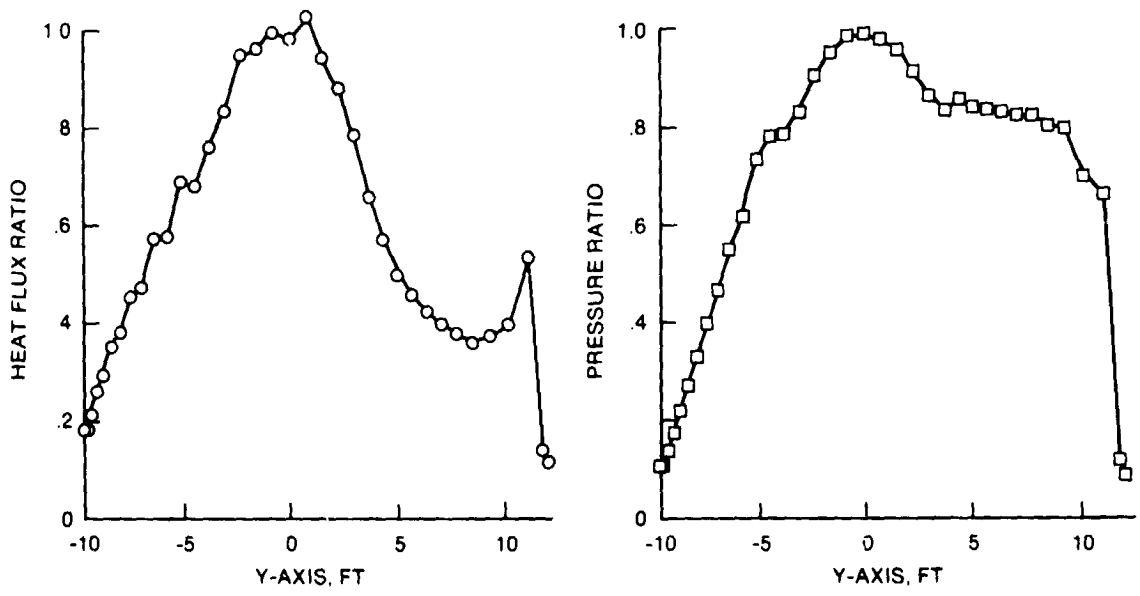


Figure 13. - Heat flux and pressure distributions on aerobrake referenced to stagnation point value.

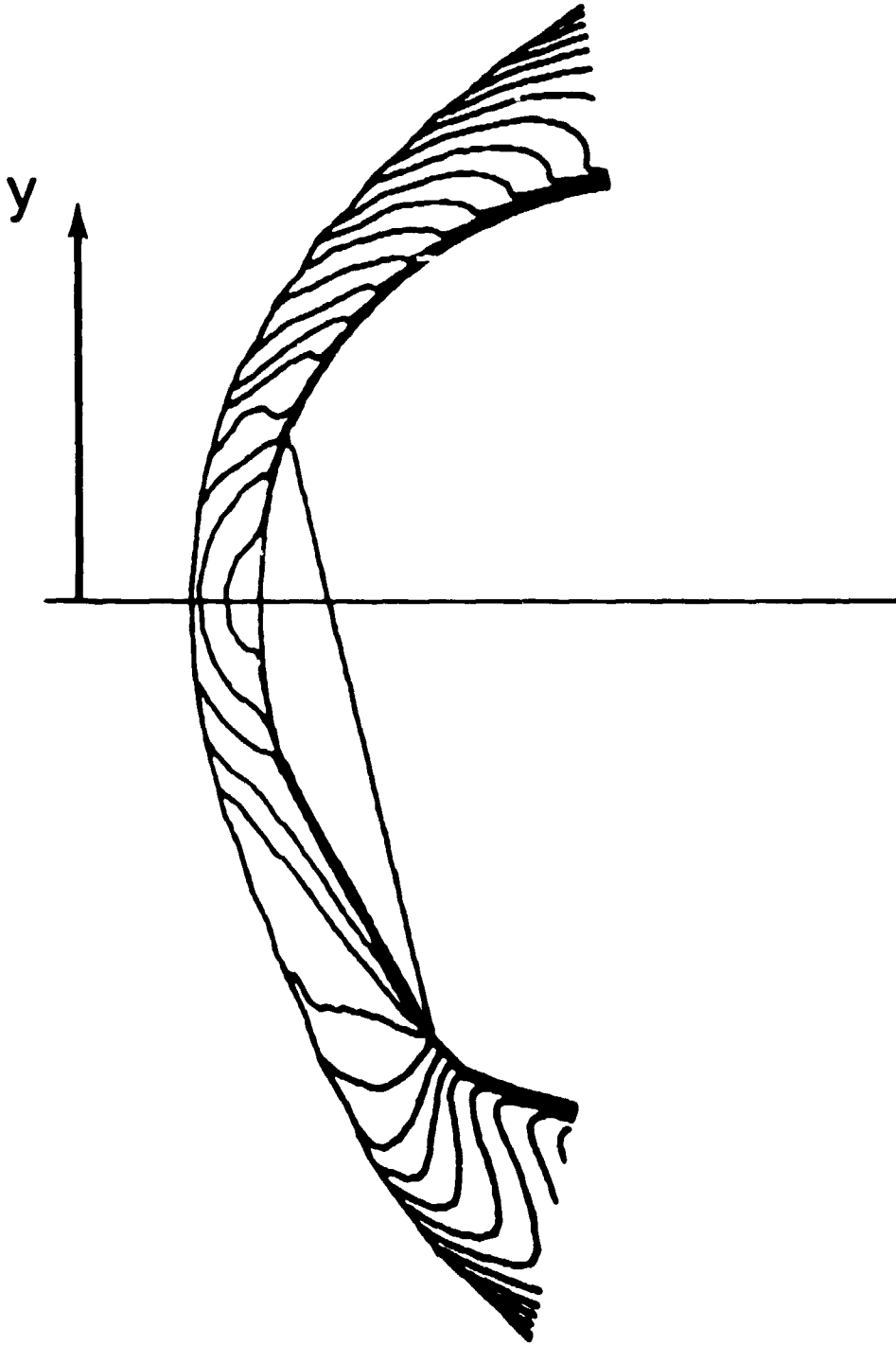


Figure 14. - Computational body with Mach number contours in shock layer.

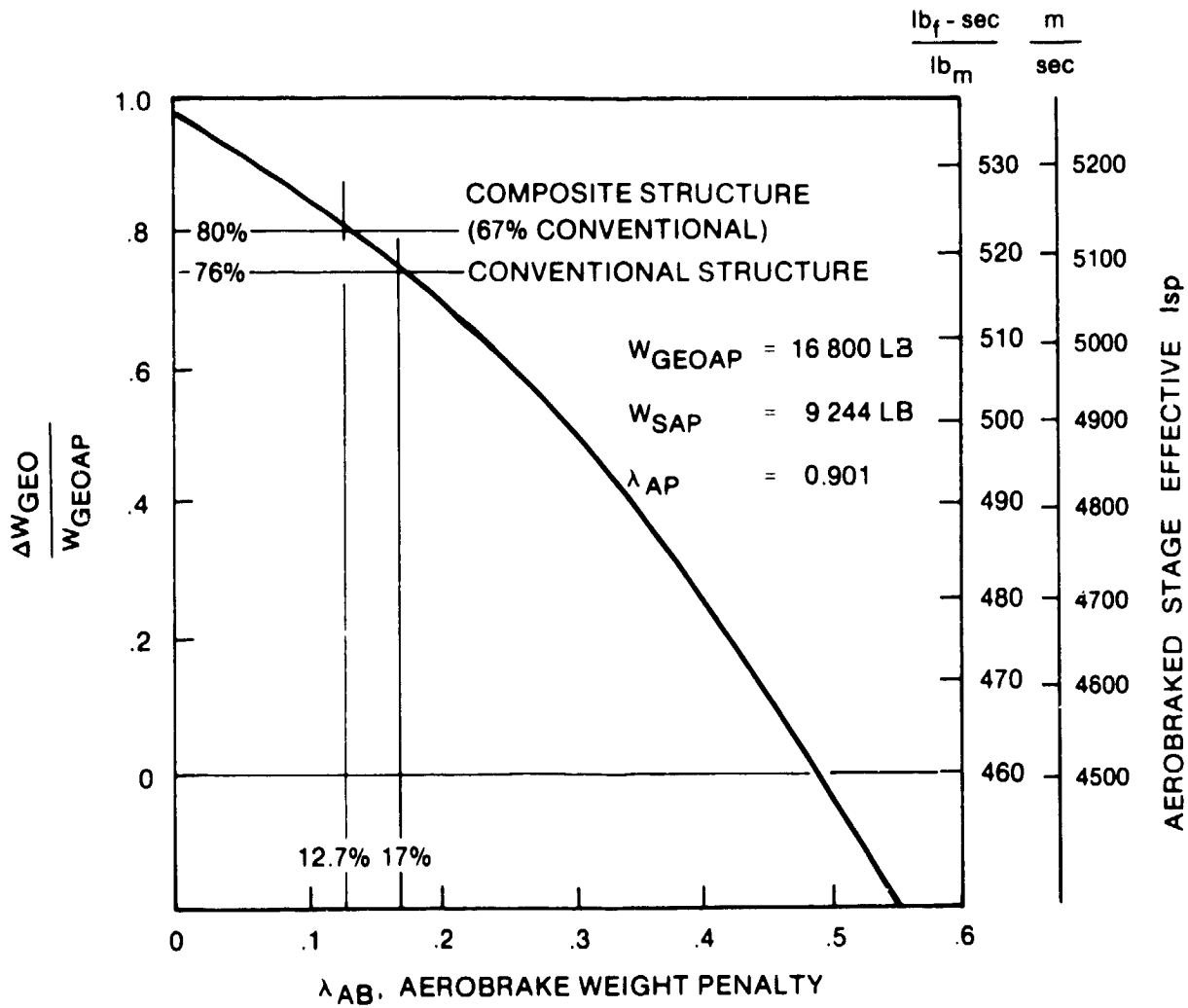


Figure 15.- Fractional increase of GEO delivery mass for aerobrakened stage over an all propulsive stage.

## REFERENCES

1. Scott, C. D.; Ried, R. C.; Marais, R. J.; Li, Chien P.; and Derry, S. M.: An AOTV Aeroheating and Thermal Protection Study. AIAA Paper 84-1710, June 1984.
2. Hethcoate, J. P.; and White, J.: Aeromaneuvering Orbit Transfer Vehicle for Space Transport System, Paper IAF-76-173 presented at XXVII Congress International Astronautical Federation (Anaheim, Calif.), Oct. 10-16, 1976.
3. Walberg, G. D.: A Review of Aeroassisted Orbit Transfer. AIAA Paper 82-1378, Aug. 1982.
4. Walberg, G. D.: Aeroassisted Orbit Transfer-Window Opens on Missions. *Astronautics & Aeronautics*, vol. 12, no. 11, Nov. 1983, pp. 36-43.
5. Andrews, D. G.; Caluori, V.A.; and Bloetscher, F.: Optimization of Aerobraked Orbital Transfer Vehicle. AIAA Paper 81-1126. Also published in *Thermodynamics of Atmospheric Entry*, AIAA Progress in Astronautics & Aeronautics, vol. 82, 1982, pp. 455-476.
6. Florence, D. E.: Aerothermodynamic Design Feasibility of a Generic Planetary Aerocapture Aeromaneuver Vehicle. AIAA Paper 81-1127. Also published in *Thermodynamics of Atmospheric Entry*, AIAA Progress in Astronautics and Aeronautics vol. 82, 1982, pp. 477-519.
7. Menees, G. P.; and Park, C.: Design and Performance Analysis of a Conical-Aerobrake Orbital Transfer Vehicle Concept. AIAA Paper 84-0410, Jan. 1984.
8. Mayo, E. E.; Lamb, R. H.; Romere P. O.: Newtonian Aerodynamics for Blunted Raked-Off Circular Cones and Raked-Off Elliptical Cones, NASA TN D-262, May 1965.
9. Gamble, J.; Cerimele, C.; Spratlin, K.: Aerobraking of a Low L/D Manned Vehicle from GEO Return to Rendezvous with the Space Shuttle, AIAA Paper 83-2110 presented at AIAA Atmospheric Flight Mechanics Conference (Gatlinburg, Tenn.), Aug. 15-17, 1983.
10. Cerimele, C.; Skalecki, L.; Gamble, J.: Meteorological Accuracy Requirements for Aerobraking Orbital Transfer Vehicles, AIAA Paper 84-0030 presented at AIAA 22nd Aerospace Sciences Meeting (Reno, Nev.), Jan. 9-12, 1984.
11. Gamble, J.; Spratlin, K.; Skalecki, L.: Lateral Directional Requirements for a Low L/D Aeromaneuvering Orbital Transfer Vehicle. AIAA Paper 84-2123 presented at AIAA Atmospheric Flight Mechanics Conference (Seattle, Wash.), Aug. 1984.

12. Ried, R. C.; Rochelle, W. C.; and Milhoan, J. D.: Radiative Heating to the Apollo Command Module: Engineering Prediction and Flight Measurement, NASA TM X-58091, Apr. 1972.
13. Li, C. P.; A Three Dimensional Navier-Stokes/Euler Code for Blunt-Body Flow Computations, AIAA Paper 85-0361 to be presented at the 23rd AIAA Aerospace Sciences Meeting (Reno, Nev.) Jan. 1985.